In Vivo Lamina Cribrosa Micro-Architecture in Healthy and Glaucomatous Eyes as Assessed by Optical Coherence Tomography

Bo Wang,[1,2] Jessica E. Nevins,[1] Zach Nadler,[1] Gadi Wollstein,[1] Hiroshi Ishikawa,[1,2] Richard A. Bilonick,[1,3] Larry Kagemann,[1,2] Ian A. Sigal,[1,2] Ireneusz Grulkowski,[4] Jonathan J. Liu,[4] Martin Kraus,[4,5] Chen D. Lu,[4] Joachim Hornegger,[5] James G. Fujimoto,[4] and Joel S. Schuman[1,2]

[1]Department of Ophthalmology, UPMC Eye Center, Eye and Ear Institute, Ophthalmology and Visual Science Research Center, University of Pittsburgh School of Medicine, Pittsburgh, Pennsylvania
[2]Department of Bioengineering, Swanson School of Engineering, University of Pittsburgh, Pittsburgh, Pennsylvania
[3]Department of Biostatistics, Graduate School of Public Health, University of Pittsburgh, Pittsburgh, Pennsylvania
[4]Department of Electrical Engineering and Computer Science, Massachusetts Institute of Technology, Cambridge, Massachusetts
[5]Department of Computer Science, University of Erlangen-Nuremberg, Nuremberg, Germany

Correspondence: Gadi Wollstein, UPMC Eye Center, 203 Lothrop Street, Suite 834, Pittsburgh, PA 15213; wollsteing@upmc.edu.

Submitted: August 21, 2013
Accepted: November 16, 2013

Citation: Wang B, Nevins JE, Nadler Z, et al. In vivo lamina cribrosa micro-architecture in healthy and glaucomatous eyes as assessed by optical coherence tomography. *Invest Ophthalmol Vis Sci*. 2013;54:8270–8274. DOI:10.1167/iovs.13-13109

Purpose. The lamina cribrosa (LC) is a prime location of glaucomatous damage. The purpose of this study was to compare LC 3-dimensional micro-architecture between healthy and glaucomatous eyes in vivo by using optical coherence tomography (OCT).

Methods. Sixty-eight eyes (19 healthy and 49 glaucomatous) from 47 subjects were scanned in a 3.5 × 3.5 × 3.64-mm volume (400 × 400 × 896 pixels) at the optic nerve head by using swept-source OCT. The LC micro-architecture parameters were measured on the visible LC by an automated segmentation algorithm. The LC parameters were compared to diagnosis and visual field mean deviation (VF MD) by using a linear mixed effects model accounting for age.

Results. The average VF MD for the healthy and glaucomatous eyes was −0.50 ± 0.80 dB and −7.84 ± 8.75 dB, respectively. Beam thickness to pore diameter ratio ($P = 0.04$) and pore diameter standard deviation ($P < 0.01$) were increased in glaucomatous eyes. With worse MD, beam thickness to pore diameter ratio ($P < 0.01$), pore diameter standard deviation ($P = 0.05$), and beam thickness ($P < 0.01$) showed a statistically significant increase while pore diameter ($P = 0.02$) showed a significant decrease. There were no significant interactions between any of the parameters and age (all $P > 0.05$).

Conclusions. Glaucomatous micro-architecture changes in the LC, detected by OCT analysis, reflect beams remodeling and axonal loss leading to reduction in pore size and increased pore size variability.

Keywords: lamina cribrosa, optical coherence tomography, glaucoma

Glaucoma is an optic neuropathy that is the second leading cause of blindness worldwide.[1] A leading target for glaucomatous damage is the lamina cribrosa (LC), a meshwork of collagen fibers through which all retinal axons pass. Previous ex vivo histologic studies on the LC have reported regional differences in areas associated with glaucomatous damage.[2–4] The authors note compression of the LC,[2] decreased pore size,[3] and elongation of pores[4] in glaucomatous eyes.

Recently, optical coherence tomography (OCT) has been used for in vivo imaging of the LC.[5] Advances in OCT technology, including deeper signal penetration and increased scanning speeds,[6] allow in vivo 3-dimensional (3D) imaging of LC at an unprecedented level of detail; the technology enables visualization of LC micro-architecture such as individual beams and pores.

However, current studies looking at in vivo LC changes in glaucoma, using OCT, have been primarily limited to analyzing *macro-architecture* features. Researchers have investigated features such as insertion points,[7] anterior surface defects,[8,9] and lamina thickness.[10] However, the 3D micro-architecture of the lamina, the collagenous support structure, and the axons passing through them have not been analyzed in vivo. Because the ganglion cell axons are passing through the entire thickness of the LC on their way to the brain, a thorough assessment of the LC for glaucoma evaluation should consider the LC in its entirety. Therefore, the purpose of this study was to examine in vivo the 3D micro-architecture features of the LC in healthy and glaucomatous eyes by using OCT.

Methods

The study was conducted in accordance with the tenets of the Declaration of Helsinki and the Health Insurance Portability and Accountability Act. The institutional review board of the University of Pittsburgh approved the study. Written informed consent was given by all subjects before participation.

Table 1. Difference in LC Micro-Architecture Between Healthy and Glaucomatous Eyes

LC Parameters	Healthy (SD)	Glaucoma (SD)	Fixed Effect (95% CI)	*P* Value
Pore count	37.0 (18.8)	57.4 (24.7)	−3.31 (−18.3, 11.7)	0.67
Pore density, pores/mm^2	80.5 (23.5)	78.6 (22.5)	3.69 (−12.6, 20.0)	0.66
Pore area, μm^2	1970 (310)	1800 (330)	94.9 (−122, 312)	0.40
Pore volume, mm^3	0.0238 (0.0161)	0.0319 (0.0183)	−0.010 (−0.001, 0.012)	0.90
Pore diameter average, μm	24.6 (2.56)	22.5 (2.3)	1.32 (−0.25, 2.88)	0.11
Pore diameter SD, μm	0.405 (0.022)	0.433 (0.022)	−0.022 (−0.036, −0.008)	<0.01
Pore aspect ratio	2.06 (0.14)	2.04 (0.11)	−0.00015 (−0.076, 0.076)	0.99
Beam thickness average, μm	46.7 (3.2)	50.0 (3.4)	−1.80 (−3.99, 0.38)	0.11
Beam thickness SD, μm	0.337 (0.013)	0.348 (0.017)	−0.0095 (−0.022, 0.0025)	0.13
Beam thickness to pore diameter ratio	1.91 (0.21)	2.25 (0.31)	−0.20 (−0.38, −0.019)	0.04
Lamina area, mm^2	0.684 (0.284)	1.220 (0.54)	−0.53 (−0.20, 0.13)	0.24
Lamina volume, mm^3	0.147 (0.071)	0.235 (0.124)	−0.098 (−0.023, 0.051)	0.54
Lamina volume fraction	0.159 (0.055)	0.143 (0.050)	0.0109 (−0.0256, 0.0474)	0.56

The fixed effect represents the linear mixed effect model of the difference between healthy and glaucomatous eyes. Positive fixed effect indicates a decrease in the parameter with disease.

Subjects

Sixty-eight eyes (19 healthy and 49 glaucomatous) of 47 subjects underwent a comprehensive ophthalmic examination of the anterior and posterior segments, intraocular pressure measurement, Swedish interactive thresholding algorithm 24-2 standard perimetry (Humphrey Field Analyzer; Zeiss, Dublin, CA), and scanning by a swept-source (SS)–OCT device, all performed in the same visit. Exclusion criteria for the study were subjects with nonglaucomatous ocular diseases, neurologic and nonglaucomatous causes for visual field damage, and intraocular surgery other than noncomplicated cataract or glaucoma surgery. Healthy eyes were characterized as having normal appearance of the optic nerve head (ONH) and retinal nerve fiber layer (RNFL), and full visual fields without any previous history of retinal diseases or glaucoma. Glaucomatous eyes were classified by clinical examination findings characteristics for glaucoma (ONH abnormality: global rim thinning, rim notch, or disc hemorrhage; RNFL defect) accompanied with typical visual field loss (reproducible glaucoma hemifield test outside normal limits). If both eyes were eligible, they were included in the appropriate category.

Image Acquisition

The SS-OCT device used in this study has a 100,000 A-scan/s scanning rate, a light source centered at 1050 nm, and a 5-μm axial resolution. This system has been previously described in detail.[11] All eyes were scanned in a 3.5 × 3.5 × 3.64-mm volume (400 × 400 × 896 pixels) centered on the ONH. Two pairs of orthogonally oriented scan volume (horizontal and vertical orientation raster scans) were obtained for each eye at a rapid succession; each pair's acquisition lasted approximately 2 seconds.

Image Processing

The two orthogonal scan volumes were registered to eliminate motion artifacts.[12] The LC was automatically segmented by using a previously described custom-built software[13] using the open-source image processing FIJI software (in the public domain at http://fiji.sc/Fiji).[14] A number of LC parameters were automatically measured within the entire visible LC (Table 1). The maximum LC volume over which beams and pores could be clearly seen was delineated and was subject to automatic segmentation using adaptive local thresholding. Pore count, pore area, pore aspect ratio (ratio of the major and minor axis) were computed by using FIJI and averaged across all C-mode slices in the 3D volume. Lamina volume was computed as the entire volume of the visible lamina, and lamina area represents the maximum intensity projection of the volume in the A-scan direction. Lamina volume fraction was computed by finding the ratio of lamina beam volume to total lamina volume. Pore area and aspect ratio were computed as their average from all C-mode scans of the LC. Pore diameter and beam thickness measurements were computed as the diameter of the largest sphere that fits within the desired structure at a given point, serving as true 3D parameters.[15]

Statistical Analysis

For a subset of eyes (n = 39) with repeated scans, a repeatability study was performed. Each scan was automatically segmented and analyzed by using the method previously described. Repeatability was determined by computing the imprecision standard deviation between the measurements from the two different scans. The adjusted imprecision standard deviation was determined by normalizing the imprecision to the measurement average.

Linear mixed effects models were constructed to assess the effect of age, clinical diagnostic group, and disease severity, using visual field mean deviation (VF MD) as a surrogate indicator, with the LC parameters. Statistical analysis was performed by using R Language and Environment for Statistical Computing program (version 2.15.1; in the public domain at http://www.R-project.org).[16] P values < 0.05 were considered statistically significant.

Results

The average age of healthy and glaucoma subjects was 40.9 ± 11.3 and 70.9 ± 9.4 years, respectively. Average VF MD was −0.50 ± 0.80 dB for healthy eyes and −7.84 ± 8.75 dB for glaucomatous eyes. A sample of C-mode slices through the LC of healthy and glaucomatous eyes is shown in Figures 1A through 1D. Differences in LC micro-architecture between glaucomatous and healthy eyes are not subjectively obvious. An example of a processed image of the LC in multiple levels of C-modes is shown in Figures 2A through 2D. to illustrate the performance of the segmentation analysis.

The automated segmentation demonstrated high reproducibility. The relative imprecision varied from 1.8% (pore diameter, pore aspect ratio, beam thickness to pore diameter ratio) to 4.17% (beam thickness SD). The only exception was pore count, which had a relative imprecision of 11.4%.

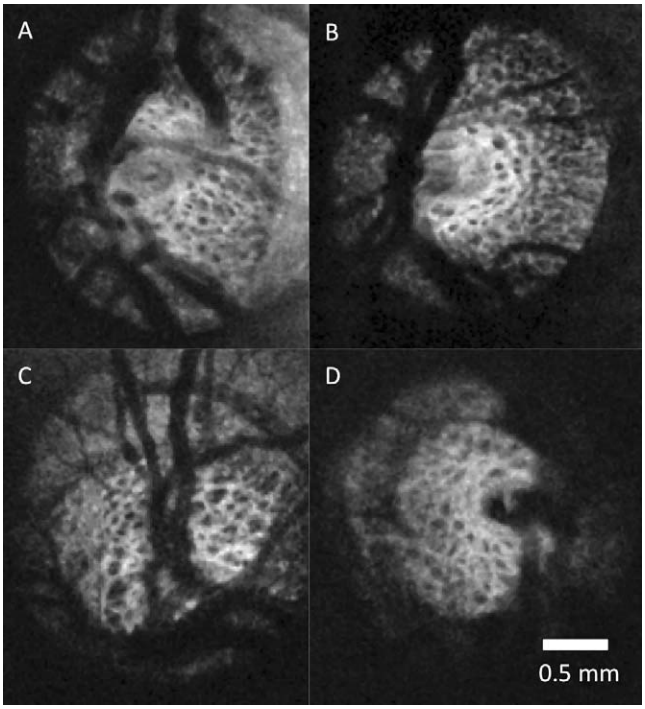

FIGURE 1. Lamina cribrosa C-mode of healthy (**A**, **B**) and glaucomatous (**C**, **D**) eyes. No systematic differences are subjectively apparent between healthy and glaucomatous eyes.

None of the LC micro-architecture parameters showed statistically significant association with age. Comparing the LC micro-architecture parameters between healthy and glaucomatous eyes, only beam thickness to pore diameter ratio and pore diameter standard deviation were statistically significantly higher in glaucomatous eyes (Table 1). However, examining the LC micro-architecture as a function of VF MD demonstrated significant relationship for several parameters (Table 2). Average beam thickness, pore diameter SD, and beam thickness to pore diameter ratio increased with worsening VF MD. Average pore diameter decreased with worsening VF MD.

DISCUSSION

In this study we quantified in vivo 3D LC micro-architecture noninvasively in healthy and glaucomatous eyes by using OCT. While most published studies are limited to assessing surface features and macroscopic characteristics, such as local surface abnormalities and total LC thickness, our study is the first to automatically quantify the LC micro-architecture in 3D.[8–10] This feature is crucial for comprehensive evaluation of glaucoma-associated changes in the LC as the axons trespassing the lamina are prone to the deleterious glaucomatous effect throughout the entire lamina. Moreover, because the micro-architecture differences between glaucoma and healthy eyes are not readily apparent (Fig. 1), an automated quantification method is required in order to identify differences that may not be obvious. Using our previously described method for automated quantification of the LC,[14] we identified several structural features that were significantly different between healthy and glaucomatous eyes.

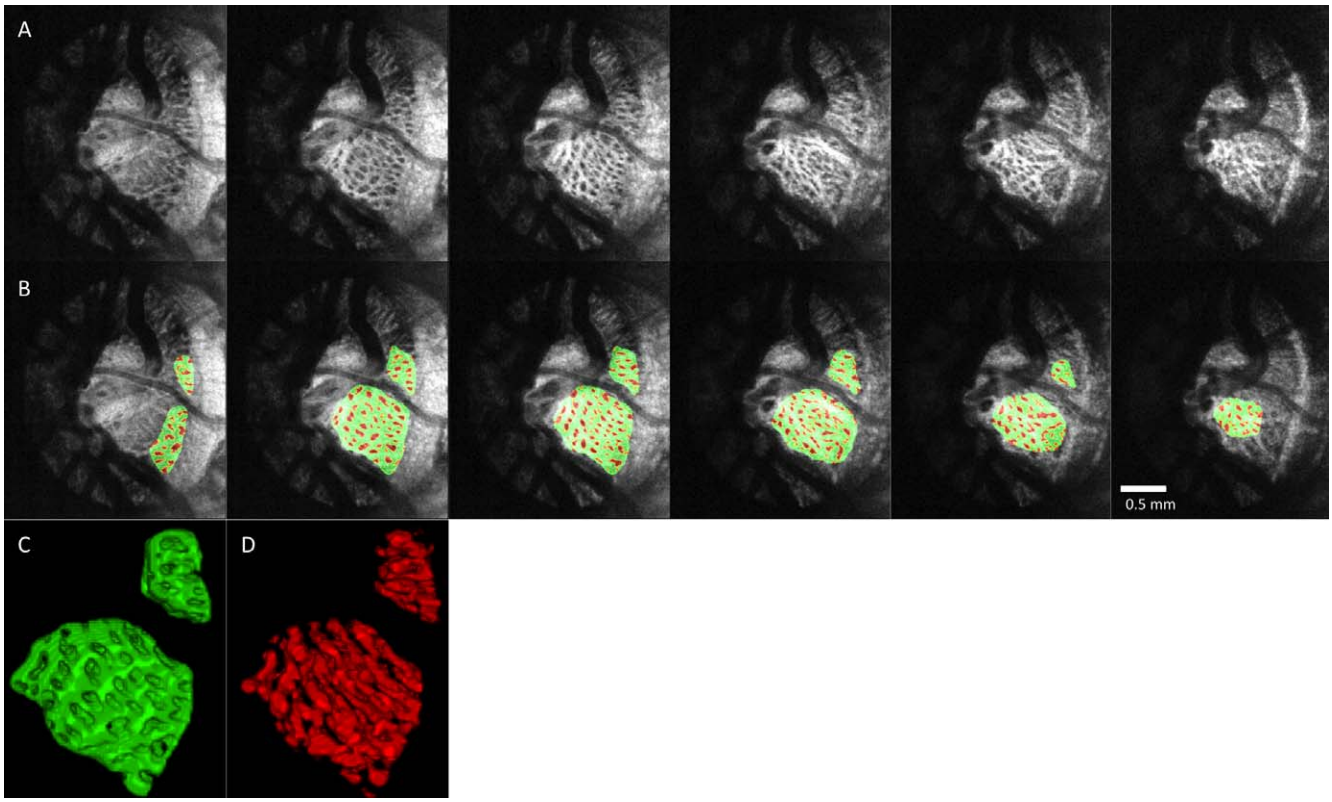

FIGURE 2. Segmentation examples. (**A**) C-mode stacks of the LC of a glaucoma subject stepping down 50-μm slices. (**B**) The same slices after segmentation with laminar beams in *green* and laminar pores in *red*. Three-dimensional reconstruction of the LC (**C**) beams and (**D**) pores.

Investigative Ophthalmology & Visual Science

Table 2. Structure-Function Relationship Between LC Micro-Architecture and VF MD

	Fixed Effect (95% CI)	*P* Value
Pore count	−1.30 (−1.89, −0.72)	<0.01
Pore density, pores/mm^2	−0.429 (−1.116, 0.258)	0.22
Pore area, μm^2	11.8 (1.5, 22.1)	0.03
Pore volume, mm^3	−0.000435 (−0.000928, 0.00005)	0.09
Pore diameter average, μm	0.0907 (0.0167, 0.1648)	0.02
Pore diameter SD, μm	−0.000731 (−0.001440, −0.000022)	0.05
Pore aspect ratio	−0.000833 (−0.004770, 0.003104)	0.67
Beam thickness average, μm	−0.162 (−0.267, −0.056)	<0.01
Beam thickness SD, μm	0.0000764 (−0.0004573, 0.0006102)	0.78
Beam thickness to pore diameter ratio	−0.0182 (−0.0266, −0.0095)	<0.01
Lamina area, mm^2	−0.0184 (−0.0323, −0.0046)	0.01
Lamina volume, mm^3	−0.00310 (−0.00653, 0.00033)	0.08
Lamina volume fraction	0.000250 (−0.001355, 0.001854)	0.76

The fixed effect represents the linear mixed effect model of change per VF MD. Positive fixed effect indicates a decrease in the parameter with worsening disease.

Reproducibility

The subset of eyes with repeated scans demonstrated excellent reproducibility, with relative imprecisions below 5%. The only exception was pore count, with an imprecision of 11.4%. This is likely caused by the fact that pore count is highly dependent on the region of LC analyzed. Poor-quality scans can substantially decrease the region of visible LC, thereby decreasing the pore count. However, the automated segmentation of the LC is robust and demonstrating excellent reproducibility.

Age-Related Changes

No LC micro-architecture parameters reached significance with respect to age. This is in agreement from prior histology and imaging work showing that although the LC stiffens with age[17] and increases in total thickness,[18] the micro-architecture is not significantly altered.[19] Detecting age-related changes may require a larger cohort of healthy eyes.

Comparing Healthy and Glaucomatous Eyes

Our data showed an association between certain LC micro-architecture and glaucoma diagnosis (Table 1). We demonstrated a significant increase in beam thickness to pore diameter ratio in glaucoma compared to healthy eyes. While these results do not show causation, the results may represent LC remodeling due to the elevated intraocular pressure, creating thicker laminar beams to distribute the increased stress. Axonal loss as well as remodeling would contribute to smaller LC pores, creating a change in beam thickness to pore diameter ratio with disease. We also observed a significant increase in pore diameter standard deviation in glaucomatous eyes. This may represent focal damage in glaucoma, causing some pores to drastically lose diameter, thus increasing the variability in pore diameter.

In our study, we did not detect a difference in pore aspect ratio between healthy and glaucoma subjects. Previous studies have reported slanted pores with increased pore aspect ratio in glaucomatous eyes as assessed by fundus photography.[3] However, fundus photography only represents a projection image; photographs are generated as the sum of all reflections along the axis of the detector. Therefore, fundus photography is not taking into account the 3D nature of the lamina. Pores traveling in a diverging or converging manner would appear elongated on projection even if they experienced no physical elongation.

Micro-Architecture Parameters and Functional Damage

Several more parameters were statistically significant when comparing micro-architecture parameters and the continuous variable of VF MD (Table 2). Similar to the results of the diagnosis analysis, both beam thickness to pore diameter ratio and pore diameter standard deviation were increased with worsening VF MD. This suggests that as disease worsens, we see progressively more remodeling in the LC, causing further beam thickening relative to pores and focal changes. The increase in pore count and lamina area with worsening VF is likely due to the exposure of the lamina in enlarged cupping with larger loss of prelaminar tissue. This likely contributed to the borderline significance in the lamina volume as well. The decrease in pore area with worsening disease reflects the shrinking pores due to axonal loss.

The use of a continuous disease severity indicator, VF MD, added two additional LC micro-architecture parameters, beam thickness and pore diameter, that were significantly related to VF MD. As the disease worsens, the pore diameter decreases and the beam thickness increases, both supporting the concept of LC remodeling in diseased eyes. The advantage of using VF MD is that we are no longer dichotomizing the study population into healthy and glaucomatous. Instead, we are able to compare LC micro-architecture with a range of disease severity and are better able to capture significant changes.

Limitations

The limitations of this study were inherent to any OCT-based analysis of the LC. Owing to shadowing from blood vessels and prelaminar tissue, the entire lamina cannot be seen on all scans. We attempted to analyze and segment as much of LC as possible, considering all regions with clearly visible LC pores and beams. However, the temporal region tends to have the largest area of visible LC and to have more weight in the analysis. Despite the temporal quadrant being less sensitive to glaucomatous damage than superior or inferior quadrants,[20] our study still had sufficient power to demonstrate significant changes in the lamina of glaucomatous eyes.

Optical coherence tomography results are not directly comparable to histology owing to differences in optical resolution and sampling density. Optical coherence tomography has significantly worse lateral resolution when compared with electron microscopy or other forms of microscopy used to study LC. Furthermore, OCT is likely to suffer from volume fraction effects; if the OCT laser beam strikes a small area of highly reflective lamina beam, the reflection would be registered as a high-intensity reflection and considered as a beam. These factors result in C-mode slices that likely overemphasize beams, compared to histology. Therefore, the LC volume fractions found in this article are higher than those reported in literature.[21] Compared to other in vivo imaging studies using scanning laser ophthalmoscopy, we found similar pore aspect ratio as well as pore area, although considerable variability exists in pore area. Our reported pore areas were closest to ones reported by Ivers et al.[22] However, Sredar et al.[23] report smaller pore areas (~1100 μm), while Akagi et al.[24] report larger values (~3000 μm). These differences are likely due to variability in segmentation algorithm used to determine pore area, as Akagi et al.[24] use manual delineation that may be

Investigative Ophthalmology & Visual Science

less likely to label smaller pores. The comparison to histology is much more difficult, since pore area can be altered by the digestion process and also fixation. Dandona et al.[25] report similar pore areas in the region of observed LC, while Jonas et al.[19] report larger areas.

Pore aspect ratio and pore area are summary measures averaging all the C-mode slices within visible lamina. Therefore, they might be considered as not true 3D parameters like pore diameter or beam thickness. Changes in the scan angle with respect to the LC may contribute to changes in pore aspect ratios and areas. We made an effort to ensure that the scan angle was always perpendicular to the ONH surface during scanning. Moreover, if the scan angle varies, the angle distribution can be expected to be similar in both healthy and glaucomatous eyes, thus neutralizing this effect.

In conclusion, we demonstrated changes in the LC microarchitecture as assessed with OCT in glaucomatous eyes. Glaucomatous eyes typically had larger beam thickness to pore diameter ratios and higher pore diameter standard deviations. Beam thickness, beam thickness to pore diameter ratio, and pore diameter standard deviation showed a statistically significant increase with worsening VF MD. Meanwhile, pore diameter decreased with worsening VF MD. These changes may represent LC remodeling and axonal loss due to glaucomatous damage.

Acknowledgments

Supported in part by National Institutes of Health Contracts R01-EY013178, R01-EY011289, P30-EY008098 (Bethesda, Maryland); Eye and Ear Foundation (Pittsburgh, Pennsylvania); Research to Prevent Blindness (New York, New York).

Disclosure: **B. Wang**, None; **J.E. Nevins**, None; **Z. Nadler**, None; **G. Wollstein**, Allergan (C); **H. Ishikawa**, None; **R.A. Bilonick**, None; **L. Kagemann**, None; **I.A. Sigal**, None; **I. Grulkowski**, None; **J.J. Liu**, None; **M. Kraus**, P; **C.D. Lu**, None; **J. Hornegger**, P; **J.G. Fujimoto**, Optovue (I), P; **J.S. Schuman**, P

References

1. Quigley HA, Broman AT. The number of people with glaucoma worldwide in 2010 and 2020. *Br J Ophthalmol*. 2006;90:262–267.
2. Quigley HA, Hohman RM, Addicks EM, Massof RW, Green WR. Morphologic changes in the lamina cribrosa correlated with neural loss in open-angle glaucoma. *Am J Ophthalmol*. 1983;95:673.
3. Tezel G, Trinkaus K, Wax MB. Alterations in the morphology of lamina cribrosa pores in glaucomatous eyes. *Br J Ophthalmol*. 2004;88:251–256.
4. Fontana L, Bhandari A, Fitzke FW, Hitchings RA. In vivo morphometry of the lamina cribrosa and its relation to visual field loss in glaucoma. *Curr Eye Res*. 1998;17:363–369.
5. Kagemann L, Ishikawa H, Wollstein G, et al. Ultrahigh-resolution spectral domain optical coherence tomography imaging of the lamina cribrosa. *Ophthalmic Surg Lasers Imaging*. 2008;39:S126–S131.
6. Choma MA, Sarunic MV, Yang C, Izatt JA. Sensitivity advantage of swept source and Fourier domain optical coherence tomography. *Opt Express*. 2003;11:2183–2189.
7. Crawford Downs J, Roberts MD, Sigal IA. Glaucomatous cupping of the lamina cribrosa: a review of the evidence for active progressive remodeling as a mechanism. *Exp Eye Res*. 2011;93:133–140.
8. Inoue R, Hangai M, Kotera Y, et al. Three-dimensional high-speed optical coherence tomography imaging of lamina cribrosa in glaucoma. *Ophthalmology*. 2009;116:214–222.
9. Lee EJ, Kim T-W, Weinreb RN, et al. Three-dimensional evaluation of the lamina cribrosa using spectral-domain optical coherence tomography in glaucoma. *Invest Ophthalmol Vis Sci*. 2012;53:198–204.
10. Park H-YL, Jeon SH, Park CK. Enhanced depth imaging detects lamina cribrosa thickness differences in normal tension glaucoma and primary open-angle glaucoma. *Ophthalmology*. 2012;119:10–20.
11. Potsaid B, Baumann B, Huang D, et al. Ultrahigh speed 1050nm swept source/Fourier domain OCT retinal and anterior segment imaging at 100,000 to 400,000 axial scans per second. *Opt Express*. 2010;18:20029–20048.
12. Kraus MF, Potsaid B, Mayer MA, et al. Motion correction in optical coherence tomography volumes on a per A-scan basis using orthogonal scan patterns. *Biomed Opt Express*. 2012;3:1182.
13. Nadler Z, Wang B, Wollstein G, et al. Automated lamina cribrosa microstructural segmentation in optical coherence tomography scans of healthy and glaucomatous eyes. *Biomed Opt Express*. In press.
14. Schindelin J, Arganda-Carreras I, Frise E, et al. Fiji: an open-source platform for biological-image analysis. *Nat Methods*. 2012;9:676–682.
15. Hildebrand T, Rüegsegger P. A new method for the model-independent assessment of thickness in three-dimensional images. *J Microsc*. 1997;185:67–75.
16. R Core Team. *R: A Language and Environment for Statistical Computing*. Vienna, Austria: R Foundation for Statistical Computing; 2013. Available at: http://www.R-project.org.
17. Albon J, Purslow PP, Karwatowski WSS, Easty DL. Age related compliance of the lamina cribrosa in human eyes. *Br J Ophthalmol*. 2000;84:318–323.
18. Kotecha A, Izadi S, Jeffery G. Age-related changes in the thickness of the human lamina cribrosa. *Br J Ophthalmol*. 2006;90:1531–1534.
19. Jonas JB, Mardin CY, Schlötzer-Schrehardt U, Naumann GO. Morphometry of the human lamina cribrosa surface. *Invest Ophthalmol Vis Sci*. 1991;32:401–405.
20. Bowd C, Zangwill LM, Berry CC, et al. Detecting early glaucoma by assessment of retinal nerve fiber layer thickness and visual function. *Invest Ophthalmol Vis Sci*. 2001;42:1993–2003.
21. Roberts MD, Grau V, Grimm J, et al. Remodeling of the connective tissue microarchitecture of the lamina cribrosa in early experimental glaucoma. *Invest Ophthalmol Vis Sci*. 2009;50:681–690.
22. Ivers KM, Li C, Patel N, et al. Reproducibility of measuring lamina cribrosa pore geometry in human and nonhuman primates with in vivo adaptive optics imaging. *Invest Ophthalmol Vis Sci*. 2011;52:5473–5480.
23. Sredar N, Ivers KM, Queener HM, Zouridakis G, Porter J. 3D modeling to characterize lamina cribrosa surface and pore geometries using in vivo images from normal and glaucomatous eyes. *Biomed Opt Express*. 2013;4:1153–1165.
24. Akagi T, Hangai M, Takayama K, Nonaka A, Ooto S, Yoshimura N. In vivo imaging of lamina cribrosa pores by adaptive optics scanning laser ophthalmoscopy. *Invest Ophthalmol Vis Sci*. 2012;53:4111–4119.
25. Dandona L, Quigley HA, Brown AE, Enger C. Quantitative regional structure of the normal human lamina cribrosa: a racial comparison. *Arch Ophthalmol*. 1990;108:393–398.

Investigative Ophthalmology & Visual Science